ACS OMEGA

Article

Cite This: ACS Omega 2019, 4, 2102−2110

http://pubs.acs.org/journal/acsodf

β-Cyclodextrin-Functionalized Cellulose Nanocrystals and Their Interactions with Surfactants

Feifei Zhang,[†] Muhammad Shahidul Islam,[†] Richard M. Berry,[‡] and Kam Chiu Tam*[,†]

[†]Department of Chemical Engineering, Waterloo Institute for Nanotechnology, University of Waterloo, 200 University Avenue West, Waterloo, Ontario N2L 3G1, Canada

[‡]CelluForce Inc., 625, Président-Kennedy Avenue, Montreal, Québec H3A 1K2, Canada

Supporting Information

ABSTRACT: β-cyclodextrin (β-CD) forms a host−guest inclusion complex with many organic and amphiphilic compounds found in pharmaceutical, textile, cosmetic, food, and personal care systems. Therefore, grafting of β-CD onto a cellulose nanocrystal (CNC) offers a possible strategy to use functionalized CNC to complex with surface-active molecules. We have successfully grafted β-CD onto CNCs in a stepwise manner using cyanuric chloride as the linker. The structure of β-CD-grafted CNC (CNC-CD) was characterized by UV−vis and Fourier-transform infrared spectroscopy, and the grafting ratio of β-CD was determined by the phenolphthalein inclusion protocol. Ionic surfactants induced the aggregation of CNC-CDs by forming inclusion complexes with β-CDs on the surface of CNC. The interactions of amphiphilic compounds with CNC-CD were examined by surface tensiometry, conductometric and potentiometric titration, and isothermal titration calorimetry. Mechanisms describing the complex formation between surfactants and CNC-CD were proposed, where an improved understanding of CD interactions with surfactants and lipids would enable better strategies for drug encapsulation and delivery with CDs.

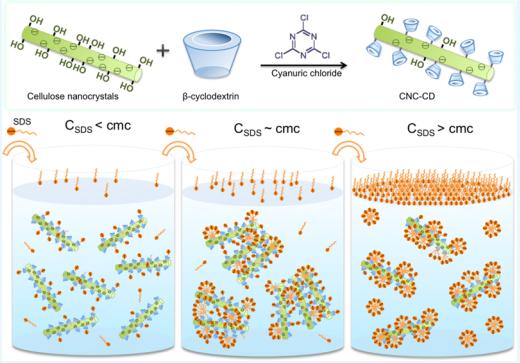

1. INTRODUCTION

Surface-active agents, also known as surfactants, are amphiphilic compounds consisting of hydrophobic and hydrophilic segments that self-assemble in water to form aggregates (micelles) beyond the critical micelle concentration (cmc). Beyond the cmc, the morphological transitions of micelles produce different morphologies, such as spheres, cylinders, vesicles, bilayers, and hexagonal phases.[1−3] These micellar structures are governed by the balance between the hydrophobic and headgroup interactions in aqueous solvents.[1] The micellar and thermodynamic properties of surfactants are mainly dependent on pH, pressure, temperature, concentration, and added electrolytes, cosurfactants, and cosolvents.[1] The specific properties, function, and application of surfactants depend on the cmc values and other parameters (the dissociation degree, aggregation number) of micellar aggregates.[1] Because of their specific properties, surfactants and their micellar systems are widely used in food formulations, detergency, drug delivery, emulsion stabilization, textiles, personal care, cosmetic products, paper and paint production, synthesis of nanomaterials, mining (flotation), as well as to generate confined and controlled reaction platforms in aqueous solutions, catalysis of organic reactions, and as mobile phases in chromatographic techniques to separate ionic and nonionic species.[1,3]

Poor aqueous solubility and rate of dissolution represent major challenges and constitute two critical factors in the formulation and delivery of drug molecules.[4] The concept of utilizing nanostructured materials with cyclodextrin (CD) for drug encapsulation has emerged as a feasible approach to improve the encapsulation and delivery of active compounds in biomedical sciences. β-Cyclodextrin (β-CD) forms a host−guest inclusion complex,[5,6] mainly driven by hydrophobic or van der Waals and hydrogen bond interactions,[4,7] with many organic and amphiphilic compounds, like surfactants found in pharmaceutical, textile, cosmetic, food, and personal care systems.[6] CDs are known to bind surfactant molecules below the surfactant cmc; however, interactions of CDs with surfactant micelles (above the cmc) are not well understood.

Cellulose is one of the most ubiquitous and abundant renewable biopolymers obtained from different sources.[8] It is a long-chain, high-molecular-weight polysaccharide (a homopolymer) composed of repeat units of dimers or disaccharides of anhydro-D-glucopyranose unit (AGU), known as cellobiose, where each AGU unit is connected by a β-1,4-glycosidic linkage.[9,10] The unique rod-shaped cellulose nanocrystal (CNC) is extracted from cellulose microfibrils by concentrated

Received: September 26, 2018
Accepted: January 10, 2019
Published: January 28, 2019

DOI: 10.1021/acsomega.8b02534
ACS Omega 2019, 4, 2102−2110

sulfuric acid-mediated hydrolysis yielding CNCs with a typical dimension ranging from 2 to 50 nm in width and 100−2000 nm in length, possessing abundant anionic sulfate ester groups onto the CNC surfaces.[8,9] Such CNCs can yield electrostatically stable colloidal dispersions,[8] and they have received an unprecedented attention in materials science because of their unique physicochemical properties.[9] The unique features of CNCs enhance their attractiveness in the development of novel functional nanomaterials and their applications,[11,12] such as additives in pharmaceuticals, personal care products, food application[13] (Pickering emulsions,[14] ice cream[15]), high-performance inorganic materials, and biomedicine (fat reduction[16]).

CDs are cyclic oligosaccharides composed of 6−8 α-D-glucopyranose units, linked by α-1,4-glucosidic linkages that form a ring and have the shape of truncated cone or torus.[5,6] They are crystalline, homogeneous, water-soluble, biocompatible, nonhygroscopic, and stable (chemically and physically) macromolecules produced by enzymatic degradation of starch.[4] Because of the presence of the primary and secondary hydroxyl groups on the exterior of the cyclic structure, the exterior of a CD is hydrophilic, which allows hydrogen bonding cohesive interactions, whereas the central cavity presents a hydrophobic environment as a host that promotes the binding interaction with hydrocarbon segments of guests (surfactants, lipids, polymers, ionic liquids, alkanes, amino acids, and vitamins) to form inclusion complexes.[5,7] Thus, nonpolar molecules or compounds are capable of displacing bound water molecules in the cavity of CD to form inclusion complexes.[17] β-CD is ideal for complexation because of its ideal cavity size, efficient drug encapsulation and loading, availability, and relatively low cost.[4] Because of its unique property in forming host−guest inclusion complexes[18−21] with a variety of nonpolar molecules, β-CD has been extensively studied and applied in medical, pharmaceutical, and health and personal care products to enhance their water solubility, stability, bioavailability, and biocompatibility of active reagents or to eliminate undesirable component from solutions.[22−24]

The design of a number of industrial formulations relies on the solution behavior of surfactants, which can be affected by the presence of various solutes. In particular, supramolecules, such as CDs, may alter the surfactant micellization in water because of host−guest interaction with the hydrophobe on the surfactant molecule.[6] Understanding the nature and characteristics of surfactant−polymer and surfactant−nanoparticle interactions is necessary to enhance the performance of many products.[25,26] In the presence of polymers, surfactants tend to aggregate on the polymer chains because of electrostatic or hydrophobic attractions at the critical aggregation concentration. In order to incorporate CNC into surfactant solutions, it is vital to understand the behavior of CNC in the presence of surfactants because of its charged characteristics. Interactions between CNC and anionic surfactants have been studied to improve the dispersibility and stability of CNC in nonpolar solvents[27] and poly (lactic acid).[28] Grafting of β-CD enables the fixation of active reagent carriers on the surface of CNC, which imparts new properties and enriches its potential applications. Surfactants, being amphiphilic molecules, can form complexes with β-CD by the inclusion of a hydrophobic segment into the nonpolar cavity. Because the surface activity and micellization behavior are significantly influenced by β-CD, a comprehensive understanding on the behavior of β-CD-grafted CNC in the presence of ionic and nonionic surfactants will facilitate the use of such nanomaterials in pharmaceuticals and personal care products. The grafting of β-CD onto magnetic-CNC was demonstrated recently by our group, and the system was used to remove organic molecules, where the host−guest inclusion of two model hydrophobic drug molecules was demonstrated.[27] In this paper, we report on the synthesis of β-CD-grafted CNC (CNC-CD) using cyanuric chloride as the linker. The reaction conditions to enhance the grafting of β-CD were examined, and Fourier transform infrared (FTIR) and UV were used to confirm the grafting. Studies on the interactions between surfactant molecules and CNC were previously reported; however, there were no studies describing the interactions between surfactants and CNC-CD. Our hypothesis is that the host−guest interaction between β-CD and various types of surfactants will impact the physical interactions with CNC-CD, and understanding of the impact of functional groups on the behavior of surfactants with modified CNC is necessary. Hence, the interactions between CNC-CD and three surfactants were investigated by microcalorimetry, surface tensiometry, conductivity, and zeta potential measurements, and the physical mechanisms describing these interactions are proposed.

2. RESULTS AND DISCUSSION

2.1. UV−Vis and FTIR. CNC-CDs synthesized in water and dimethyl sulfoxide (DMSO) were characterized by UV−vis (Figure 1) and FTIR spectroscopy (Figure 2). Mono-

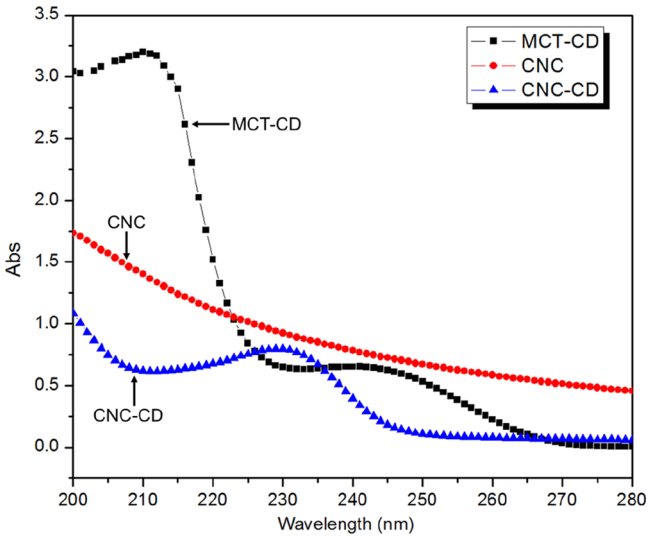

Figure 1. UV−vis spectra of MCT-β-CD, CNC, and CNC-CD.

chlorotriazine (MCT)-β-CD possessed a specific absorbance at 245 nm, and upon the substitution of the third chlorine atom, the change in the electron distribution on the triazine ring induced a blue shift from 245 to 230 nm. Pristine CNC did not display any specific UV absorbance, and the observed absorbance without any peaks was attributed to scattering from the CNC nanorods.

The FTIR spectra of cyanuric chloride and MCT-β-CD are compared in Figure 2, where the peaks centered at 1579 and 1467 cm^{-1} are attributed to the triazine ring on the cyanuric chloride. The peaks between 1487 and 868 cm^{-1} are the characteristic bands for β-CD molecules. In addition, the new peak at 819 cm^{-1} is attributed to C−Cl bond that has red-

DOI: 10.1021/acsomega.8b02534
ACS Omega 2019, 4, 2102−2110

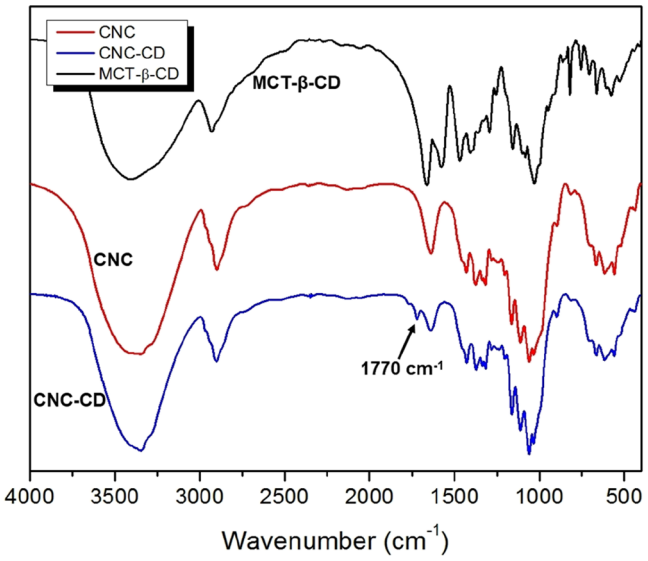

Figure 2. FTIR spectra of CNC, CNC-CD, and MCT-β-CD synthesized in water.

shifted from 920 nm^{-1} because of the substitution of chlorine atoms.[29]

The spectra of CNC-β-CD (water) and CNC-β-CD (DMSO) both possessed new peaks at 1722 and 1770 cm^{-1}, which are attributed to C═O stretching from the rearrangement of triazine rings as shown in Scheme S1.[30]

2.2. Grafting Ratio of MCT-β-CD. Phenolphthalein (PHTH) molecules deprotonate and form a 1:1 host−guest inclusion complex with β-CD above a pH of 8.2. Free PHTHs in the bulk phase possess a UV absorption peak at 552 nm, whereas those forming an inclusion complex with β-CD no longer absorb at this wavelength. With the increasing β-CD concentration, the pink color of PHTH solutions gradually faded and the absorbance of PHTH solutions decreased proportionally, which yields a linear relationship between ln(Abs of PHTH) and ln(β-CD concentration) (Figures S1 and S2). Because pristine CNC is negatively charged due to the sulfate groups on its surface (reported sulfur content, S = 0.86%),[31,32] PHTH did not interact electrostatically with pristine CNC. The amounts of PHTH molecules included in the cavity of β-CD could be used to determine the weight percentage of β-CD in CNC-CD.

The grafting ratio of β-CD on CNC depends on the reaction conditions and the solvent environment (Figure S3). For the reaction in water and DMSO, the average grafting ratios of β-CD were 3.32 and 4.92 wt %, respectively. The observed difference is related to the hydrolysis of chlorine atoms on MCT-β-CD, which reduced the reactivity with the hydroxyl groups on CNC. By reducing the water content in the reaction, the β-CD grafting ratio was enhanced, but it was still lower than when using DMSO as the solvent, indicating that water content is critical in the reactions with cyanuric chloride.

In addition to the impact of water, the hydrolysis of chlorine atoms on MCT-β-CD was affected by the concentration of sodium bicarbonate, reaction temperature, and time. Sodium bicarbonate was used to scavenge hydrogen chloride (HCl) molecules generated from −Cl substitution and the hydrolysis of −Cl from the added base. The grafting ratio was enhanced by increasing the reaction temperature and reducing the heating time with an upper limit of 140 °C, beyond which β-CD started to degrade and CNC began to discolor and become yellowish.

The reaction conditions for the use of cyanuric chloride as a linker to graft β-CD on CNC were optimized. In comparison to a previous study,[33] where CNC was labeled with 5-(4,6-dichlorotriazinyl)aminofluorescein (5-DTAF), our grafting ratio was approximately 10^3 times (29.7 μmol/g) better than 5-DTAF (24 ± 1 nmol/g) despite the molecular weight of β-CD being much larger than that of 5-DTAF.

2.3. Interactions with a Nonionic Surfactant. Surface tension and enthalpy changes of a nonionic surfactant, 4-octylphenol polyethoxylate (TX-100) in water, CD, CNC suspension, and CNC-CD suspension were measured as a function of TX-100 concentration (Figure 3A). TX-100

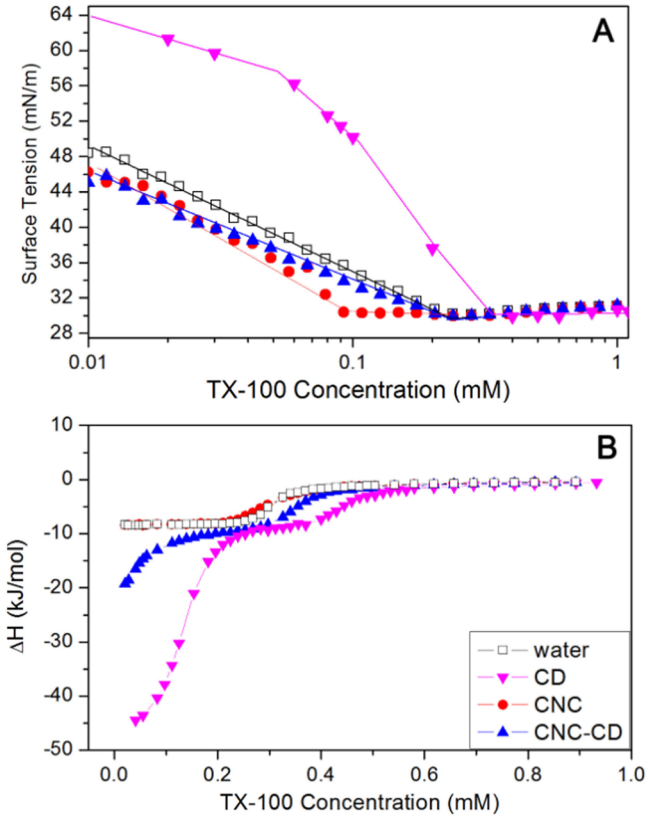

Figure 3. (A) Surface tension curves of water, 0.6 wt % CNC, and 0.6 wt % CNC-CD suspensions with increasing TX-100 concentrations at 25 °C and (B) thermograms from titrating TX-100 into water, 0.18 mM β-CD, 0.6 wt % CNC, and 0.6 wt % CNC-CD suspensions at 25 °C.

possessed a cmc of 0.28 mM in water as determined from the inflexion point of surface tension and the first-order differential curve of the isothermal titration calorimetry (ITC) thermogram (Figure S4). The surface tension of TX-100 in a CNC suspension did not change much up to the inflexion point at 0.09 mM, where it started to decrease. This is attributed to the hydrophilic tail of TX-100 that possibly hydrogen-bonded to the hydroxyl groups on the surface of CNC, whereas the hydrophobic domains remained surface-active and partitioned to the air−water interface (Scheme 1-top left panel). Because CNC is much larger than TX-100 molecules, the interface became saturated more rapidly at a lower TX-100 concentration. The calculated surface area coverage was larger compared with TX-100 alone (given by the

DOI: 10.1021/acsomega.8b02534
ACS Omega 2019, 4, 2102−2110

Scheme 1. Schematic Diagrams Describing the Changes in the Behavior of CNC-CD Compared to CNC in Different Charged Surfactants[a]

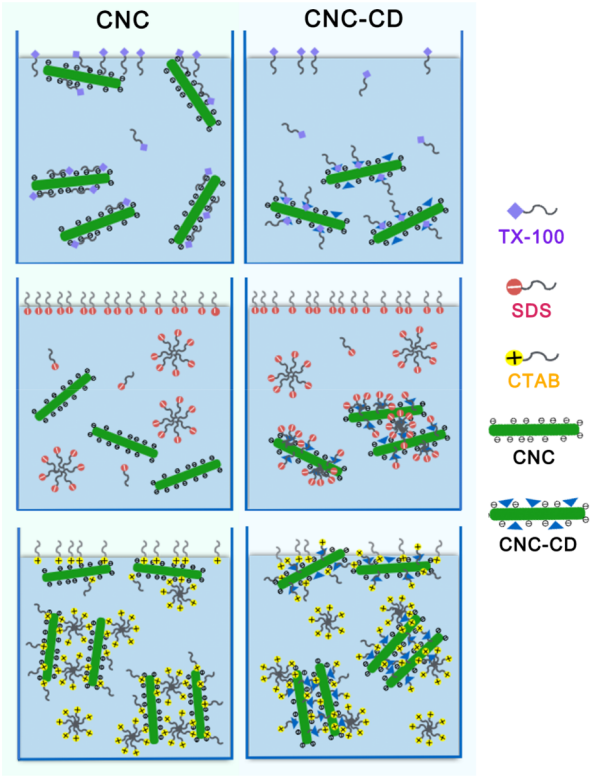

[a]The concentration shown in the scheme is below the cmc for TX-100 and above the cmc for SDS and CTAB.

slope of surface tension vs ln(c) in Figure 3A), signifying that the TX-100/CNC aggregates occupied a larger surface area at the air−water interface. However, the behavior of TX-100 in the CNC-CD suspension was different; the surface tension in CNC-CD decreased slower than in water, indicating a reduced surface activity of TX-100 at the same concentration. This can be explained by the hydrophobic segment of TX-100 forming a host−guest inclusion complex with β-CD, resulting in a loss in its surface activity by the detachment from the interface and partitioning to the bulk solution (Scheme 1-top right panel). The identical cmc observed for TX-100 in water and CNC-CD is possibly due to a higher affinity of TX-100 monomers for the air−water interface than to β-CD.

From the calorimetric curves of TX-100 (Figure 3B), the difference between titrations into water and into CNC suspension was negligible. However, the ITC thermograms of the TX-100/CNC-CD system revealed a large exothermic enthalpy change at very low TX-100 concentration, which was also observed in the TX-100/CD system. This confirmed the host−guest interaction between TX-100 and β-CD as postulated earlier from the surface tension data. The shift of the cmc to a higher value for both CNC-CD and β-CD was attributed to the inclusion complexation of TX-100 monomers and β-CD, thus more monomers were required to produce the micelles.

2.4. Interactions with an Anionic Surfactant. In the surface tension measurements (Figure 4A), the slopes [$d\gamma$/$d\ln(c)$] (designated as slope 1) prior to the cmc for the addition of sodium dodecyl sulfate (SDS) into water, CNC

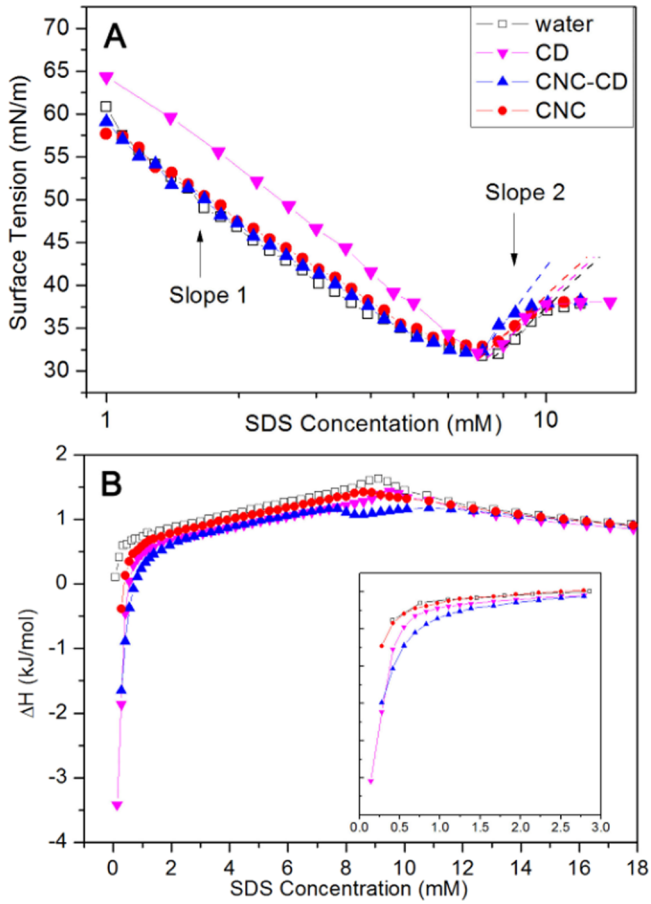

Figure 4. (A) Surface tension curves of water, 0.6 wt % CNC, and 0.6 wt % CNC-CD suspensions with increasing SDS concentrations at 25 °C. (B) Thermograms from titrating SDS into water, 0.18 mM β-CD, 0.6 wt % CNC, and 0.6 wt % CNC-CD suspensions at 25 °C. The inset is an enlargement of the region at low SDS concentration.

suspension, and CNC-CD suspension were identical, and only slope 2 for CNC-CD (after the cmc) was different. The valley in the surface tension curve is due to trace contaminants arising from SDS synthesis or from the hydrolytic reaction, which were frequently observed in studies on the surface activity of SDS. In the presence of the hydrophobic cavity of β-CD in the bulk phase, the removal of contaminants from the air−water interface was facilitated by the inclusion complexation phenomenon, resulting in a more rapid recovery of the surface tension for the CNC-CD system.

In the ITC thermogram for the SDS titration into CNC-CD, an exothermic interaction at low concentration was observed, which was similar to the titration into β-CD, confirming the inclusion activity of β-CD toward SDS monomers after it had been grafted on the CNC surface. In the concentration range of 7.4−10.8 mM, an obvious deviation in enthalpy change for the SDS/CNC-CD system was observed (Figure 4B). This exothermic interaction can likely be attributed to the inclusion complex-induced aggregation of SDS.

To gain a clearer understanding of this interaction, transmittance and zeta potential were measured and compared with the ITC results (Figure 5). The zeta potential of CNC-CD was less negative than that of pristine CNC because of the partial hydrolysis of sulfate groups during the grafting reaction. With increasing SDS concentration, CNC displayed a gradual increase in the zeta potential, whereas CNC-CD showed an

DOI: 10.1021/acsomega.8b02534
ACS Omega 2019, 4, 2102−2110

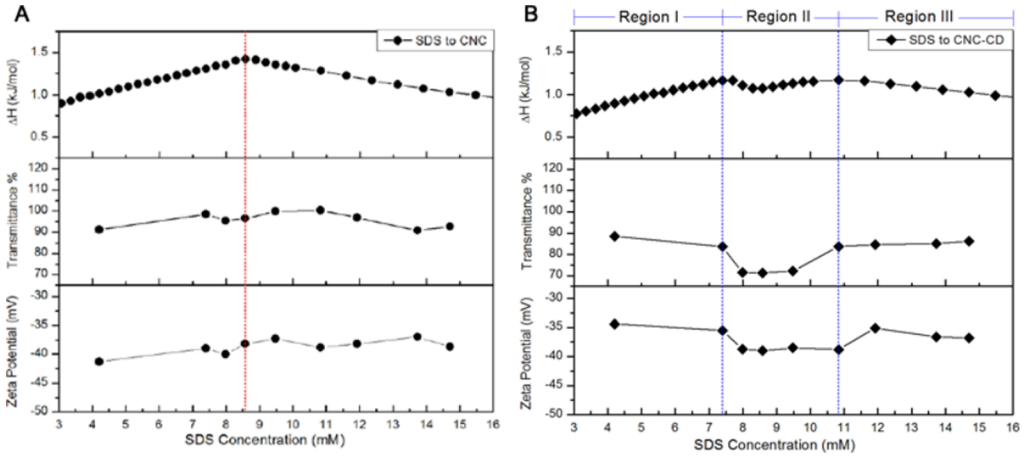

Figure 5. Comparison of ITC, transmittance, and zeta potential results for CNC/SDS (A) and CNC-CD/SDS (B) samples.

initial reduction up to region II and then a slight increase at 10.8 mM. The formation of a host−guest complex between SDS and CNC-CD could be responsible for the drop in the zeta potential because of the increased negative charge on CNC-CD. From transmittance measurements, SDS/CNC showed no obvious changes after the cmc, whereas CNC-CD became slightly cloudy in region II, indicating the appearance of larger sized particles because of the agglomeration of SDS-bound CNC-CD induced by hydrophobic interactions between free and partially bound C_{12} alkyl chains (Scheme 1-middle right panel). In the photos taken under natural light, light scattering particles were evident in the SDS/CNC-CD samples of region II and disappeared at higher SDS concentration. The SDS/CNC samples remained translucent over the entire region (Figure S5). Conductivity measurements for the addition of SDS to CNC-CD also showed three regions (Figure S6). In region II, a lower conductivity observed in the SDS/CNC-CD suspension suggested a reduced mobility of SDS monomers in the bulk because of the encapsulation of SDS monomers on β-CD grafted on CNC.

TEM images of SDS/CNC and SDS/CNC-CD revealed the aggregation of SDS induced by the inclusion complex on the surface of CNC-CD (Figure 6). The CNC and CNC-CD concentrations were kept low to avoid the agglomeration of CNC-CD observed in region II. From the images, both CNC and CNC-CD were well dispersed, whereas the aggregation of SDS was only observed on the nanorods of CNC-CD. In summary, at the SDS concentration in region II, CNC did not interact with SDS monomers or micelles. With CNC-CD, aggregates, induced by the formation of SDS/β-CD host−guest complexes on the surface of CNC, were formed at an SDS concentration of ∼7.6 mM and dissociated at ∼10.8 mM. In the SDS/β-CD host−guest complexes, because of the length of the C12 alkyl chains and the length of the CD cavity, part of the hydrophobic chains was exposed. When the SDS concentration was increased, the monomers nucleated around the inclusion complex driven by hydrophobic forces; this is a different mechanism than the polymer-induced aggregation of the surfactant. Considering the size of the aggregates, it is highly likely that the aggregation of free or included SDS monomers could bridge with other SDS/CNC-CD complexes to form larger aggregates, which were then visible to the naked eyes. Beyond the cmc (∼11 mM), the SDS aggregates on the CNC-CD complexes continued to grow, leading to the dissociation of large SDS/CNC-CD aggregates to form smaller stable SDS/CNC-CD nanorods in water.

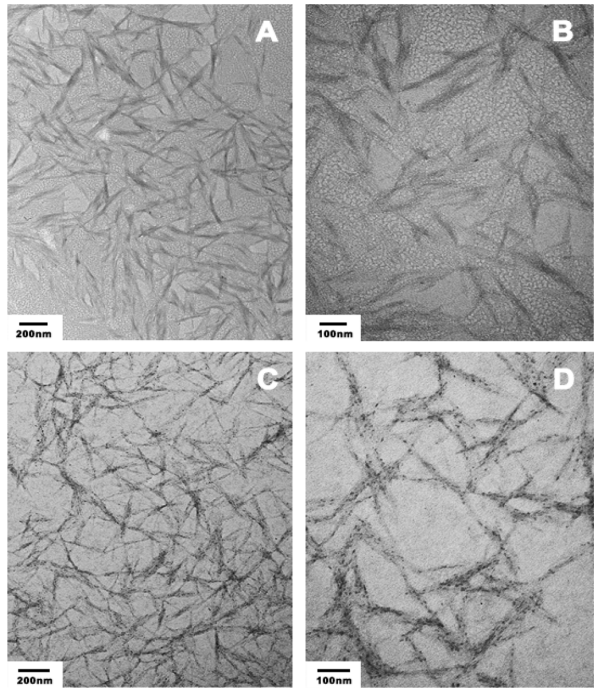

Figure 6. Transmission electron microscopy (TEM) images of 0.02 wt % of CNC (A,B) and CNC-CD (C,D) with 8.5 mM SDS.

2.5. Interactions with a Cationic Surfactant. The cmc of hexadecyl-trimethyl-ammonium bromide (CTAB) in water is ∼1 mM as evident from the inflection point in the surface tension (Figure 7A) and the first-order differential curve of the ITC data. With CNC and CNC-CD suspensions, changes in the surface tension followed a similar trend, but they were different from the CTAB/water curve. The surface tension profile could be divided into three regions with different slopes. In the region with slope 1, positively charged groups on the CTAB monomers were bound to the negatively charged CNC surface and remained in the bulk solution.[34] Only a small fraction of the CTAB monomers were partitioned to the air−water interface as confirmed by the slower reduction in the surface tension. Because the hydrophobic tails of CTAB monomers bound to the CNC were exposed to the bulk water, with an increasing number of bound monomers, CNC particles

DOI: 10.1021/acsomega.8b02534
ACS Omega 2019, 4, 2102−2110

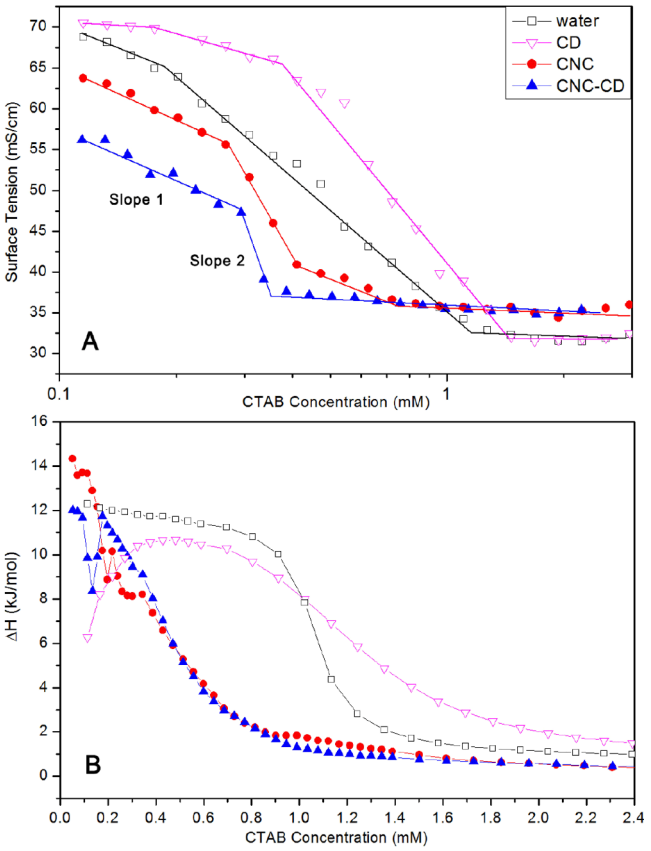

Figure 7. (A) Surface tension curves of water, 0.1 wt % CNC, and 0.1 wt % CNC-CD suspensions with increasing CTAB concentrations at 28 °C and (B) thermograms of titrating SDS to water, 0.03 mM β-CD, 0.1 wt % CNC, and 0.1 wt % CNC-CD suspensions at 28 °C.

became more hydrophobic and aggregated (Scheme 1-bottom left panel).[34] At the first inflection point on the curve, CNCs were driven to the interface by hydrophobic forces, resulting in a rapid drop in surface tension with slope 2. The surface tension of CNC-CD was lower than that of CNC but decreased at the same rate as in slope 1. This could be explained by the reduced negative charge of CNC-CD, where more CTAB monomers were driven to the air−water interface. The host−guest interactions between CTAB hydrophobic tails and grafted β-CD promoted the bridging of CNC-CDs to form large hydrophobic aggregates that rise to the air−water interface, which reduced the surface tension as shown in the region with slope 2 (Scheme 1-bottom right panel).

The host−guest interaction between CTAB and β-CD was described by a smaller ΔH at low concentration as seen in the ITC thermogram (Figure 7B). A similar reduction was also observed when CNC-CD was compared to CNC in the region where the electrostatic and host−guest interactions both contributed to the ΔH. At ∼0.2 mM in CNC-CD and ∼0.3 mM in CNC, the slight increase in the ΔH is attributed to the aggregation of CNC or CNC-CD particles in the bulk that correspond to the reduced slope in the conductivity (Figure S7). Because of the bridging effect of the CTAB/β-CD complex, aggregation of CNC-CDs occurs at a lower concentration.

Comparison of the calorimetric, phase separation, and zeta potential results provided a comprehensive understanding on the aggregation behavior of CNC and CNC-CD in the presence of CTAB (Figure 8). In region I, the zeta potential increased slowly when bound CTAB monomers adsorbed the CNC and CNC-CD nanoparticles that produced small amounts of precipitates. At the onset of region II, CNC-CDs were bridged by CTAB, inducing a rapid aggregation and a faster precipitation, resulting in a less negative zeta potential. The second reduction in the column height of the precipitates at 0.25 mM CTAB corresponded to denser aggregates that settled into a more compressed structure because of the further increase in the zeta potential to ∼0 mV. At the end of region II, the microstructure of the aggregates became less compact because of the continuous binding of CTAB molecules that dissociated the aggregates into smaller, relatively better-dispersed aggregates, yielding an increase in the height of the aggregates in region III. However, it was not possible for CTAB to entirely disperse CNC or CNC-CD nanoparticles to form transparent suspensions even at concentration above the cmc. The difference in CTAB-induced precipitation of CNC and CNC-CD can be observed in Figure S8.

3. CONCLUSIONS

β-CDs were successfully grafted to CNC, where the grafting ratio of β-CD was determined by the PHTH inclusion method. The interactions between CNC-CD nanoparticles and TX-100,

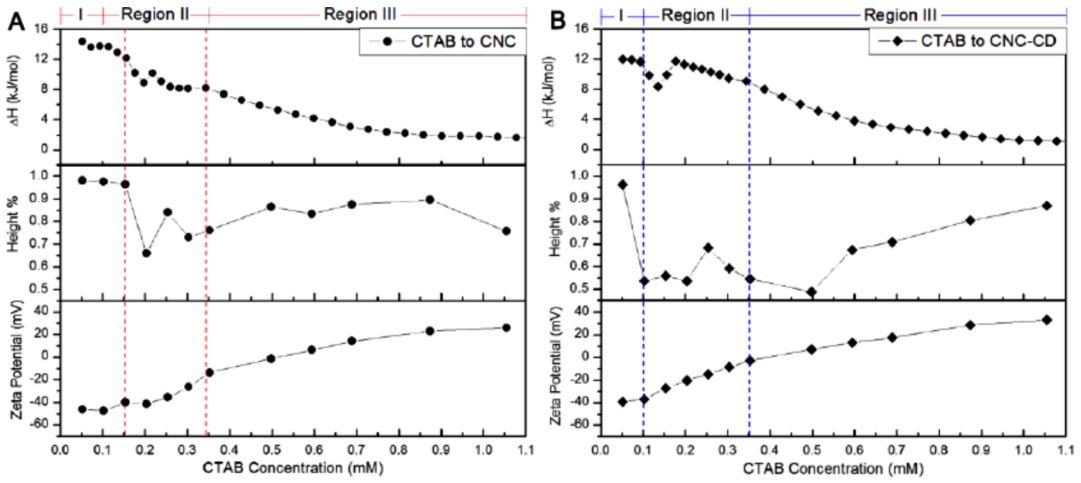

Figure 8. Comparison of ITC, height %, and zeta potential results for CNC/CTAB (A) and CNC-CD/CTAB (B) samples.

DOI: 10.1021/acsomega.8b02534
ACS Omega 2019, 4, 2102−2110

SDS, and CTAB were investigated by surface tensiometry, ITC, conductometry, transmittance, phase separation, and zeta potential measurements. The primary interactions in the CNC-CD/TX-100 and CNC-CD/SDS systems are host−guest interactions between the hydrophobic domain of surfactants and β-CD. Inclusion complex-induced aggregation was also observed in CNC-CD/SDS, probably due to the incomplete inclusion of the SDS alkyl chain. Both host−guest and electrostatic interactions between positively charged CTAB and negatively charged CNC-CD contributed to the formation of precipitates and the transition from loose to compact aggregates.

4. EXPERIMENTAL SECTION

4.1. Materials. Spray-dried CNCs were supplied by CelluForce Inc. CNC suspensions were prepared by vigorous mixing using a 500 W IKA T-25 homogenizer, followed by sonication in a 700 W 42 kHz Branson sonication bath. Cyanuric chloride, β-CD hydrate (99%), PHTH, TX-100, SDS (>99%), and CTAB (>99%) were purchased from Sigma-Aldrich and used as received. Deionized Millipore water was used for all the sample preparations.

4.2. Synthesis. The synthesis of MCT-β-CD was conducted according to the procedure reported by Liu et al.[35] A clear solution of dichlorotriazine sodium salt was obtained by dispersing cyanuric chloride in a NaOH solution in an ice bath for 1 h. β-CD solution at pH 12 was then added to allow the reaction between the primary hydroxyl groups on CNC and dichlorotriazine at a temperature of 10 °C until the pH became neutral (Schemes 2 and S1). MCT-β-CD was

Scheme 2. Procedure for MCT-β-CD Synthesis

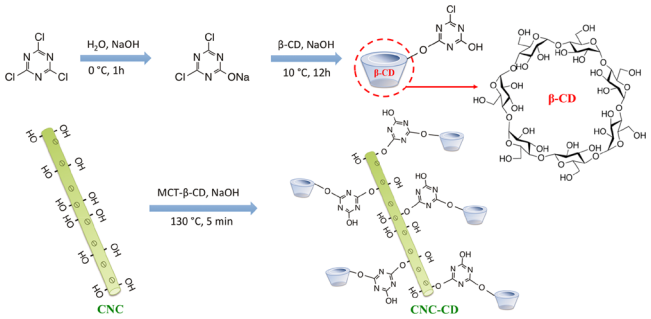

purified using acetone and DMF with repetitive precipitation. Finally, the product was filtered and dried in a vacuum oven until a constant weight was achieved.

The optimum reaction conditions for the synthesis of β-CD-grafted CNCs (CNC-CD) were determined. CNC concentration, sodium bicarbonate content, heating temperature, and time were all found to have an influence on the β-CD grafting ratio. In the optimized procedure, a 2 wt % suspension of CNC was first activated in 0.02 w/w $NaCO_3$ solution for 3 h, followed by the addition of various amounts of MCT-β-CD at room temperature. The water content in the mixture was then reduced to around 10 wt % on a Heidolph Laborota 4011 rotating evaporator at 45 °C. The grafting reaction was conducted by heating the concentrated mixture at 130 °C for 5 min. Unreacted MCT-β-CD molecules were removed by dialysis against water over 2 weeks. CNC-CD in DMSO was also synthesized, and the procedure is described in the Supporting Information.

4.3. Spectroscopy. Ultraviolet absorbance of cyanuric chloride, CNC, and CNC-CD was measured on a Varian (Carey 100 Bio) UV−visible spectrometer at room temperature. Transmittance was also measured on the same instrument at 600 nm. FTIR spectra of samples in compressed KBr powder were obtained on a Bio-Rad (Excalibur series) FTIR spectrometer over scanning wavelengths of 400−4000 cm^{-1}.

4.4. Transmission Electron Microscopy. TEM images were taken on a Philip CM10 electron microscopy to visualize the inclusion complex-induced SDS aggregates on the surface of CNC-CD. The TEM samples were prepared by depositing one drop of 0.02 wt % suspension onto a carbon-coated copper grid. Samples with surfactants were prepared by placing copper grids on a filter paper and excess liquid was removed by the filter paper, and the dried nanoparticles were retained for analysis.

4.5. Grafting Ratio. The grafting ratio of β-CD was measured by the PHTH inclusion method. Freshly prepared solution of 0.1 mM PHTH in 0.02 M $NaCO_3$ buffer was used for all the measurements. CNC-CD suspensions were mixed with PHTH, stirred, and equilibrated overnight before measuring the absorbance of the solutions. Samples without PHTH were also prepared as blank controls. The amount of β-CD was determined by a calibration of log(absorbance of PHTH/β-CD mixture) against log(concentration of β-CD). The grafting ratio was then determined from eq 1

$$\text{Grafting ratio} = \frac{C(\beta\text{-CD})}{C(\text{CNC-CD})} \times 100\% \quad (1)$$

4.6. Surface Tensiometry. Surface tension measurements were conducted on a DCAT 11 (DataPhysics) tensiometer. Continuous dosing was performed by a liquid dispensing unit that is capable of dosing microliters of titrants. The Wilhelmy plate method was used to measure the dynamic surface tension at the air−water interface. A total of 2 mM TX-100 and 30 mM SDS were titrated into 40 mL of water and CNC and CNC-CD suspensions at 25 °C respectively. CTAB (5 mM) was titrated into 40 mL of water and CNC and CNC-CD suspensions at 28 °C. In this paper, the concentration of CNC and CNC-CD suspensions was 0.6 wt % for interactions with TX-100 and SDS and 0.1 wt % for the interaction with CTAB.

4.7. Isothermal Titration Calorimetry. The interactions between CNC, CNC-CD, and surfactants were studied using the MicroCal VP-ITC instrument. Stock solutions of 100 mM SDS, 5 mM TX-100, and 10 mM CTAB were prepared in advance and loaded to a 282 μL syringe. CNC and CNC-CD suspensions with concentrations described above were loaded to the 1.455 mL sample cell. The titrants were injected into the sample cell at predetermined volumes of 1−10 μL in each injection. The enthalpy change of the interactions was measured and reported in kJ/mol of the injectant and plotted against surfactant concentration.

4.8. Zeta Potential. Mixtures of surfactant and CNC or CNC-CD suspensions were prepared at selected surfactant concentrations described on the ITC thermograms. Zeta potential measurements were conducted in polystyrene cuvettes on a Malvern Zetasizer Nano ZS90. The samples were sonicated and measured without dilution. This method was used to determine the overall surface charge of CNC and CNC-CD samples in the presence of ionic surfactants.

DOI: 10.1021/acsomega.8b02534
ACS Omega 2019, 4, 2102−2110

4.9. Phase Separation. Coacervation and phase separation behavior were observed and examined in CTAB/CNC and CTAB/CNC-CD samples. All samples were mixed and stabilized for 2 weeks prior to the measurements. The height of the flocculation column was normalized to the height of the total solution column with each sample for ease of comparison.

4.10. Conductivity. The conductivity measurements were performed on the Metrohm 809 Titrando System equipped with Tiamo software, which can dose microliters of the titrant in each injection. All the measurements were conducted in a jacketed vessel with a stirring speed of 4. The same temperature and concentrations of surfactants and CNC and CNC-CD suspensions were used as in surface tension measurements. The conductivity was measured using a conductivity electrode.

■ ASSOCIATED CONTENT

Supporting Information

The Supporting Information is available free of charge on the ACS Publications website at DOI: 10.1021/acsomega.8b02534.

Synthesis, determination of β-CD grafting on CNC, photographs of the complexes formed, analysis of the interactions of surfactants with β-CD-CNC using ITC, and conductometric titration (PDF)

■ AUTHOR INFORMATION

Corresponding Author

*E-mail: mkctam@uwaterloo.ca. Phone: 1-519-888-4567 ext. 38339. Fax: 1-519-888-4347.

ORCID

Kam Chiu Tam: 0000-0002-7603-5635

Notes

The authors declare no competing financial interest.

■ ACKNOWLEDGMENTS

We wish to acknowledge CelluForce Inc. for providing the CNCs. The research funding from CelluForce and FP Innovations facilitated the research on CNC. K.C.T. wishes to acknowledge funding from CFI and NSERC.

■ REFERENCES

(1) Jakubowska, A.; Pawlak, M. Determination of Physicochemical Parameters of Sodium Dodecyl Sulfate in Aqueous Micellar Solutions Containing Short-Chain Alcohols. *J. Chem. Eng. Data* **2018**, *63*, 3285−3296.

(2) Shah, S. K.; Chatterjee, S. K.; Bhattarai, A. Micellization of cationic surfactants in alcohol—water mixed solvent media. *J. Mol. Liq.* **2016**, *222*, 906−914.

(3) Vierros, S.; Sammalkorpi, M. Effects of 1-hexanol on C12E10 micelles: a molecular simulations and light scattering study. *Phys. Chem. Chem. Phys.* **2018**, *20*, 6287−6298.

(4) Gidwani, B.; Vyas, A. A Comprehensive Review on Cyclodextrin-Based Carriers for Delivery of Chemotherapeutic Cytotoxic Anticancer Drugs. *BioMed Res. Int.* **2015**, *2015*, 1−15.

(5) Jia, H.; Leng, X.; Zhang, D.; Lian, P.; Liang, Y.; Wu, H.; Huang, P.; Liu, J.; Zhou, H. Facilely Control the SDS Ability to Reduce the Interfacial Tension via the Host-Guest Recognition. *J. Mol. Liq.* **2018**, *255*, 370−374.

(6) Tsianou, M.; Fajalia, A. I. Cyclodextrins and Surfactants in Aqueous Solution above the Critical Micelle Concentration: Where Are the Cyclodextrins Located? *Langmuir* **2014**, *30*, 13754−13764.

(7) Lavoine, N.; Tabary, N.; Desloges, I.; Martel, B.; Bras, J. Controlled release of chlorhexidine digluconate using β-cyclodextrin and microfibrillated cellulose. *Colloids Surf., B* **2014**, *121*, 196−205.

(8) Peng, B.; Tang, J.; Wang, P.; Luo, J.; Xiao, P.; Lin, Y.; Tam, K. C. Rheological Properties of Cellulose Nanocrystal-Polymeric Systems. *Cellulose* **2018**, *25*, 3229−3240.

(9) Islam, M. S.; Chen, L.; Sisler, J.; Tam, K. C. Cellulose Nanocrystal (CNC)−Inorganic Hybrid Systems: Synthesis, Properties and Applications. *J. Mater. Chem. B* **2018**, *6*, 864−883.

(10) Mohammed, N.; Grishkewich, N.; Tam, K. C. Cellulose Nanomaterials: Promising Sustainable Nanomaterials for Application in Water/Wastewater Treatment Processes. *Environ. Sci.: Nano* **2018**, *5*, 623−658.

(11) Tang, J.; Sisler, J.; Grishkewich, N.; Tam, K. C. Functionalization of Cellulose Nanocrystals for Advanced Applications. *J. Colloid Interface Sci.* **2017**, *494*, 397−409.

(12) Grishkewich, N.; Mohammed, N.; Tang, J.; Tam, K. C. Recent Advances in the Application of Cellulose Nanocrystals. *Curr. Opin. Colloid Interface Sci.* **2017**, *29*, 32−45.

(13) Khan, A.; Wen, Y.; Huq, T.; Ni, Y. Cellulosic Nanomaterials in Food and Nutraceutical Applications: A Review. *J. Agric. Food Chem.* **2018**, *66*, 8−19.

(14) Tang, J.; Quinlan, P. J.; Tam, K. C. Stimuli-Responsive Pickering Emulsions: Recent Advances and Potential Applications. *Soft Matter* **2015**, *11*, 3512−3529.

(15) Velásquez-Cock, J.; Serpa, A.; Vélez, L.; Gañán, P.; Gómez Hoyos, C.; Castro, C.; Duizer, L.; Goff, H. D.; Zuluaga, R. Influence of Cellulose Nanofibrils on the Structural Elements of Ice Cream. *Food Hydrocolloids* **2019**, *87*, 204−213.

(16) DeLoid, G. M.; Sohal, I. S.; Lorente, L. R.; Molina, R. M.; Pyrgiotakis, G.; Stevanovic, A.; Zhang, R.; McClements, D. J.; Geitner, N. K.; Bousfield, D. W.; et al. Reducing Intestinal Digestion and Absorption of Fat Using a Nature-Derived Biopolymer: Interference of Triglyceride Hydrolysis by Nanocellulose. *ACS Nano* **2018**, *12*, 6469−6479.

(17) Del Valle, E. M. M. Cyclodextrins and Their Uses: A Review. *Process Biochem.* **2004**, *39*, 1033−1046.

(18) Valente, A. J. M.; Söderman, O. The Formation of Host−Guest Complexes between Surfactants and Cyclodextrins. *Adv. Colloid Interface Sci.* **2014**, *205*, 156−176.

(19) Hu, Q.-D.; Tang, G.-P.; Chu, P. K. Cyclodextrin-Based Host-Guest Supramolecular Nanoparticles for Delivery: From Design to Applications. *Acc. Chem. Res.* **2014**, *47*, 2017−2025.

(20) Karoyo, A. H.; Borisov, A. S.; Wilson, L. D.; Hazendonk, P. Formation of Host-Guest Complexes of β-Cyclodextrin and Perfluorooctanoic Acid. *J. Phys. Chem. B* **2011**, *115*, 9511−9527.

(21) Auletta, T.; de Jong, M. R.; Mulder, A.; van Veggel, F. C. J. M.; Huskens, J.; Reinhoudt, D. N.; Zou, S.; Zapotoczny, S.; Schönherr, H.; Vancso, G. J.; et al. β-Cyclodextrin Host−Guest Complexes Probed under Thermodynamic Equilibrium: Thermodynamics and AFM Force Spectroscopy. *J. Am. Chem. Soc.* **2004**, *126*, 1577−1584.

(22) Eastburn, S. D.; Tao, B. Y. Applications of Modified Cyclodextrins. *Biotechnol. Adv.* **1994**, *12*, 325−339.

(23) Cal, K.; Centkowska, K. Use of Cyclodextrins in Topical Formulations: Practical Aspects. *Eur. J. Pharm. Biopharm.* **2008**, *68*, 467−478.

(24) Marques, H. M. C. A Review on Cyclodextrin Encapsulation of Essential Oils and Volatiles. *Flavour Fragrance J.* **2010**, *25*, 313−326.

(25) Goddard, E. D. Polymer/surfactant interaction-Its relevance to detergent systems. *J. Am. Oil Chem. Soc.* **1994**, *71*, 1−16.

(26) Tam, K. C.; Wyn-Jones, E. Insights on Polymer Surfactant Complex Structures during the Binding of Surfactants to Polymers as Measured by Equilibrium and Structural Techniques. *Chem. Soc. Rev.* **2006**, *35*, 693−709.

(27) Heux, L.; Chauve, G.; Bonini, C. Nonflocculating and Chiral-Nematic Self-Ordering of Cellulose Microcrystals Suspensions in Nonpolar Solvents. *Langmuir* **2000**, *16*, 8210−8212.

DOI: 10.1021/acsomega.8b02534
ACS Omega 2019, 4, 2102−2110

(28) Bondeson, D.; Oksman, K. Dispersion and Characteristics of Surfactant Modified Cellulose Whiskers Nanocomposites. *Compos. Interfaces* **2007**, *14*, 617−630.
(29) Ibrahim, N. A.; Abdalla, W. A.; El-Zairy, E. M. R.; Khalil, H. M. Utilization of monochloro-triazine β-cyclodextrin for enhancing printability and functionality of wool. *Carbohydr. Polym.* **2013**, *92*, 1520−1529.
(30) Kamiński, Z. J. Triazine-Based Condensing Reagents. *Biopolymers* **2000**, *55*, 140−164.
(31) Reid, M. S.; Villalobos, M.; Cranston, E. D. Benchmarking Cellulose Nanocrystals: From the Laboratory to Industrial Production. *Langmuir* **2017**, *33*, 1583−1598.
(32) Akhlaghi, S. P.; Zaman, M.; Mohammed, N.; Brinatti, C.; Batmaz, R.; Berry, R.; Loh, W.; Tam, K. C. Synthesis of Amine Functionalized Cellulose Nanocrystals: Optimization and Characterization. *Carbohydr. Res.* **2015**, *409*, 48−55.
(33) Abitbol, T.; Palermo, A.; Moran-Mirabal, J. M.; Cranston, E. D. Fluorescent Labeling and Characterization of Cellulose Nanocrystals with Varying Charge Contents. *Biomacromolecules* **2013**, *14*, 3278−3284.
(34) Brinatti, C.; Huang, J.; Berry, R. M.; Tam, K. C.; Loh, W. Structural and Energetic Studies on the Interaction of Cationic Surfactants and Cellulose Nanocrystals. *Langmuir* **2016**, *32* (3), 689−698.
(35) Liu, J. H.; Xu, H. C.; Shen, L.; Chen, R. Y.; Yu, Z. C. Synthesis of Monochlorotriazinyl-β-Cyclodextrin as a Novel Textile Auxiliary. *Adv. Mater. Res.* **2012**, *441*, 431−435.

DOI: 10.1021/acsomega.8b02534
ACS Omega 2019, 4, 2102−2110